Liu *et al. Energy Mater* 2023;3:300028
DOI: 10.20517/energymater.2023.05

Energy Materials

Review

Open Access

Check for updates

Advanced 3D-structured electrode for potassium metal anodes

Dongqing Liu[1], Jun Shen[1], Zelang Jian[2], Xingke Cai[3,*]

[1] College of Mechatronics and Control Engineering, Shenzhen University, Shenzhen 518060, Guangdong, China.
[2] School of Material Science and Engineering, Wuhan University of Technology, Wuhan 430070, Hubei, China.
[3] Institute for Advanced Study, Shenzhen University, Shenzhen 518060, Guangdong, China.

***Correspondence to:** Prof. Xingke Cai, Institute for Advanced Study, Shenzhen University, No. 3688, Nanhai Avenue, Shenzhen 518060, Guangdong, China. E-mail: cai.xingke@szu.edu.cn

How to cite this article: Liu D, Shen J, Jian Z, Cai X. Advanced 3D-structured electrode for potassium metal anodes. *Energy Mater* 2023;3:300028. https://dx.doi.org/10.20517/energymater.2023.05

Received: 6 Feb 2023 **First Decision:** 21 Mar 2023 **Revised:** 31 Mar 2023 **Accepted:** 21 Apr 2023 **Published:** 3 Jul 2023

Academic Editors: Federico Bella, Wei Tang **Copy Editor:** Fangyuan Liu **Production Editor:** Fangyuan Liu

Abstract

The potassium (K) metal anode, following the "Holy Grail" Li metal anode, is one of the most promising anode materials for next-generation batteries. In comparison with Li, K exhibits even more pronounced energy storage properties. However, it suffers from similar challenges as most alkali metal anodes, such as safety and cyclability issues. Borrowing strategies from Li/Na metal anodes, the three-dimensional (3D)-structured current collector has proven to be a universal and effective strategy. This study examines the recent research progress of 3D-structured electrodes for K metal anodes, focusing on the most commonly used host materials, including carbon-, metal-, and MXene-related electrode materials. Finally, existing challenges, various perspectives on the rational design of K metal anodes, and the future development of K batteries are presented.

Keywords: Potassium metal anode, 3D-structured electrode, metal batteries, current collectors

INTRODUCTION

Efficient utilization of devices and the development of various methods for storing energy are crucial to the functioning of society[1-3]. Since the first launch of C/$LiCoO_2$ rocking batteries by Sony in 1991, lithium-ion batteries (LIBs) have developed rapidly and are gradually being applied in our daily lives. Over the past three decades, LIBs have developed significantly, accounting for more than 60% of the global battery

market[4]. With the broad application of LIBs in portable electronic devices and electric vehicles, they require higher energy density, better sustainability, and larger scalability[5,6]. However, commercial LIBs using transition metal oxide cathodes and graphite anodes can hardly meet these requirements as they approach their energy density limit of 300 Wh kg^{-1}[7]. Various promising alternatives have been proposed, such as sulfur (S) and O_2 for the cathode[8,9] and alkali metals [Li, Na, and potassium (K)] for the anode[10,11]. Among the alkali metallic alternatives for graphite anodes, Li metal anodes exhibit more advanced properties, including a higher theoretical capacity [3,860 (Li) *vs.* 1,166 (Na) and 685 (K) mAh g^{-1}] and lower redox potential [-3.040 (Li) *vs.* -2.714 (Na) and -2.930 V (K)] than Na and K[12,13]. However, compared to Na and K, Li metal suffers from the shortcomings of scarce resources, inhomogeneous distribution, and high cost[14-16]. Therefore, Na and K metal anodes have emerged as promising candidates for next-generation batteries.

Advantages of K metal anodes: Potassium-ion batteries (PIBs) were first introduced in 2004 by Eftekhari and have garnered considerable research interest ever since[17]. Even though PIBs are still in their infancy, significant research efforts have been devoted to electrode material design, electrolyte optimization, and better configurations[18-22]. With significantly higher energy density, the use of K metal anodes in PIBs holds great promise, similar to Li/Na metal anodes for lithium/sodium-ion batteries[23,24]. The specific strengths of the K metal anode can be identified as follows[18,25,26]: abundant resources distributed globally (K: 2.09 wt.% *vs.* Li: 0.0017 wt.%), cost-effective raw materials (K_2CO_3), reduced production cost and weight (owing to the use of an Al current collector), improved K^+ ionic transportation kinetics (with lower desolation energy and higher ionic conductivity), environmental friendliness, and sustainability (without the use of cobalt).

Challenges of K anodes: Although K metal anodes offer several advantages, their development undoubtedly faces significant challenges, as is the case with most alkali metal anodes owing to long-term cyclability and safety issues. These two major problems mainly originate from the ultrahigh reactivity of alkaline metals and significant volume changes during plating/stripping[24,27]. More specifically, the highly reactive alkali-metals react with the electrolyte spontaneously to form an unstable and fragile solid electrolyte interface (SEI); the SEI easily fractures with variances in volume during plating/stripping, resulting in the exposure of fresh metal surface, repeated consumption of electrolyte, and formation of new SEI and "dead" alkali-metals. These issues not only lead to low coulombic efficiency (CE) and poor cycle life but also causes dendrites initiation/growth and separator penetration, inducing short-circuit and thermal runaway[26,28,29]. For K metal anodes, these problems can be more severe than those for Li or Na metal anodes because of their intrinsically higher reactivity and more significant volume changes during cycling.

Strategies for developing K metal anodes: To solve the problems associated with K metal anodes, extensive research has been conducted by borrowing ideas from Li and Na metal anodes. The strategies for obtaining high-performance Li metal anodes can be roughly divided into three major categories: electrolyte regulation, interface modification, and anode design[30-33]. Electrolyte regulation can be partially categorized as interface modification, as it aims to improve the quality of SEI films[34]. The commonly used electrolytes for K metal anodes include liquid- and solid-state electrolytes. The liquid electrolyte regulation strategy includes the addition of additives, changing solvents, or using multifunctional salts. These electrolyte modification methods can improve the quality of the naturally formed fragile SEI, boost its robustness, and prevent unwanted side reactions between the K metal anode and the electrolyte. In addition, a well-formed SEI can regulate the ion flux and guide uniform K metal deposition. The high reactivity of K metal anodes necessitates greater consideration of safety issues, which can be addressed by employing non-flammable electrolytes as a viable solution. However, the selection of suitable solvents for K metal anodes is difficult because of their ultrahigh chemical reactivity and further investigation is required to identify viable options.

In addition to liquid electrolytes, solid electrolytes exhibiting higher safety, thermal stability, and mechanical strength are also capable of stabilizing K metal anodes. However, solid-state electrolytes also have challenges that need to be solved, such as low ionic conductivity and low stability of the electrode/SEI. This has been summarized in previously published reviews[35-38]. In addition, interface modification, including artificial SEI construction, has also been used to avoid the disadvantages of electrolyte-reduced films[39,40]. An ideal SEI film after interfacial modification should be electronically insulating and highly ionic conductive for uniform and improved ionic diffusion and mechanically strong to withstand dendrite initiation and volume fluctuation[41-43].

Secondly, the anode design is usually concerned with the construction of a three-dimensional (3D) host to decrease the local current density, increase the lithium deposition area, guide uniform ionic flux, provide sufficient space to accommodate the deposited lithium, and maintain mechanical stability to buffer volumetric fluctuations[27,30,44-47]. Moreover, the surface of a 3D matrix can be modified with alkaliphilic materials, such as secondary phases or heteroatom doping, to decrease the nucleation barrier, provide more nucleation sites, and guide uniform alkali metal growth[48]. In addition to the above-mentioned strategies, several other effective methods have been proposed, such as alkali-metal-based alloys[49], separator modification[50-52], advanced characterization tool exploration[53], and regulation of cell operation conditions[27].

3D-structured electrode: Among the proposed methods, a 3D porous current collector has proven to be a universal and effective method for synthesizing alkali metal anodes, which directly influences the initial alkali metal nucleation and subsequent growth process. Specifically, the structural features of a 3D current collector can homogenize the electronic/ionic distribution, provide sufficient space for metal accommodation, and effectively suppress dendrite formation. The advantages of 3D porous current collectors are apparent when compared to planar current collectors. First, the 3D porous current collectors with large specific surface areas can reduce the local current density and postpone the initiation of lithium dendrite growth. Second, the 3D current collector can also regulate the homogenous ion flux, facilitate electrolyte penetration, and reduce the polarization induced by the ionic concentration. In contrast, 2D current collectors with high current densities can easily cause uneven charge distribution, surface protuberances, and dendrite growth. Third, the porous host is capable of accommodating volumetric changes during plating/dissolution rather than the large volume expansion of the planar current collector. Fourth, the highly porous structure is effective in releasing the stress generated during deposition and avoiding the occurrence of whiskers, mosses, or dendrites. Moreover, the well-developed synthetic techniques of obtaining 3D porous structures promote the rapid development of alkali metal anodes with such structures. Therefore, extensive research has been conducted regarding Li metal anodes, including fabrication methods, microstructure construction, and functional design, which have been previously reviewed in detail[28,54].

For the rational design of K metal anodes, they should be robust enough to survive long-term cyclic processes, possess excellent electronic/ionic conductive matrices to ensure efficient charge transport kinetics, provide sufficient space for K accommodation, and make better use of low-cost raw materials and cost-effective synthesis processes[55,56]. Usually, the 3D host of the K metal anode is encapsulated with metallic K to form a K composite electrode, and the commonly applied methods include thermal infusion, electrochemical deposition, and mechanical pressing[55,57]. In recent years, there has been a growing research interest and progress in K metal batteries and K metal anodes. However, few studies focused on the 3D-structured electrode for K metal anodes. This paper first introduces the research background/application prospects and advantages/challenges of K metal anodes, followed by effective strategies

accumulated from Li/Na metal anode studies and the popular anode design approach of 3D-structured electrodes. Subsequently, recent advances in 3D structure electrodes for K metal anode applications are comprehensively reviewed, mainly categorized into carbon-based, metal-based (Cu, Al, and alloy), and MXene-related electrodes, as shown in Figure 1. In addition, the surface of a 3D anode is usually covered with K-affinity materials as nucleation sites. They work synthetically with the high specific surface area of the 3D hosts and a facilitated charge-transport network to improve the overall electrochemical performance. Finally, recent developments in 3D K metal anodes are summarized, and perspectives for future investigations are proposed.

CARBON-BASED ELECTRODE MATERIALS

Carbonaceous materials exhibit several advantageous properties, such as low density, low cost, high electrical conductivity, high (structural, dimensional, and electrochemical) stability, multiple structures, excellent flexibility, and adjustable properties, and various synthesis methods are widely applied for the modified current collectors of alkaline metal anodes, especially the carbon materials fabricated into 3D architecture[28,30,44,57]. The 3D structure and surface chemistry can be tuned to regulate the electrochemical performance. Taking Li metal anodes as an example, there is a variety of 3D morphologic carbon-based electrode materials, such as interconnected carbon nanotubes[58], carbon fiber cloth (paper)[59], and graphene frameworks[60]. To induce homogeneous lithium deposition, carbon-based current collectors are commonly modified with lithiophilic functional groups, such as nitrogen (N)-[61], oxygen-[62], heteroatom-doped materials[63], and metal-based nanoparticles[64,65].

To realize stable and uniform K deposition on K metal anodes, Li *et al.* implanted an alkali metal affinitive metal oxide NiO in a carbon-based material-puffed millet (PM) through a pore-formation reaction[66]. In Figure 2A, the PM has a macroporous structure (80 μm) with small pores on the macropore wall (50 nm) and evenly distributed NiO in the pores (30 nm). The as-formed well-knit root structure, denoted as PM/NiO, had an increased surface area, which decreased charge accumulation. More importantly, the evenly distributed NiO not only served as a K nucleation site but also reacted with K and strongly connected K with the substrate. The initial deposition of K on PM/NiO and the strength between them are important for its electrochemical performance, as they can determine further deposition processes and electrode stability. Consequently, the PM/NiO/K symmetric cells cycled at 0.4 mA cm^{-2} exhibit stable voltage polarization for 200 cycles; the CEs of PM/NiO/K-based cells increase with increasing cycles and reach 99.8% after 200 cycles. The full cell assembled with a K Prussian blue ($K_{0.220}Fe[Fe(CN)_6]_{0.805}$) cathode exhibited both high rate capability and long-term cyclic stability, with an initial discharge capacity of 160 mAh g^{-1} and capacity retention of 82% after 160 cycles, which are significantly better than those of the Cu/K-based cells.

The construction of mixed electronic and ionic conducting networks using stable and conductive hosts has been approved for use in Li and Na metal anodes. A commonly applied strategy involves accommodating Li or Na in a conductive host via melt infusion or electrodeposition. For K metal anodes, Qin *et al.* infused the molten K into the aligned carbon nanotube membrane (ACM) to construct 3D conductive K-ACM anodes[67]. During the preparation process shown in Figure 2B, liquid K was infused into the ACM host quickly, presenting a golden color owing to the strong capillary forces of the ACM. The pristine aligned structure of ACM was maintained, and metallic K was uniformly distributed in the 3D ACM framework. The as-prepared 3D K-ACM host improved the electrode/electrolyte interactions and constructed efficient electron and ionic pathways [Figure 2B]. Consequently, the K-ACM symmetric cells cycled at current densities of 1.0, 2.0, and 5.0 mA cm^{-2} exhibited long-term stability of 14,000, 10,000, and 3,500 h with small overpotentials of 0.1, 0.13, and 0.31 V, respectively, which was significantly better than those of K cells. The

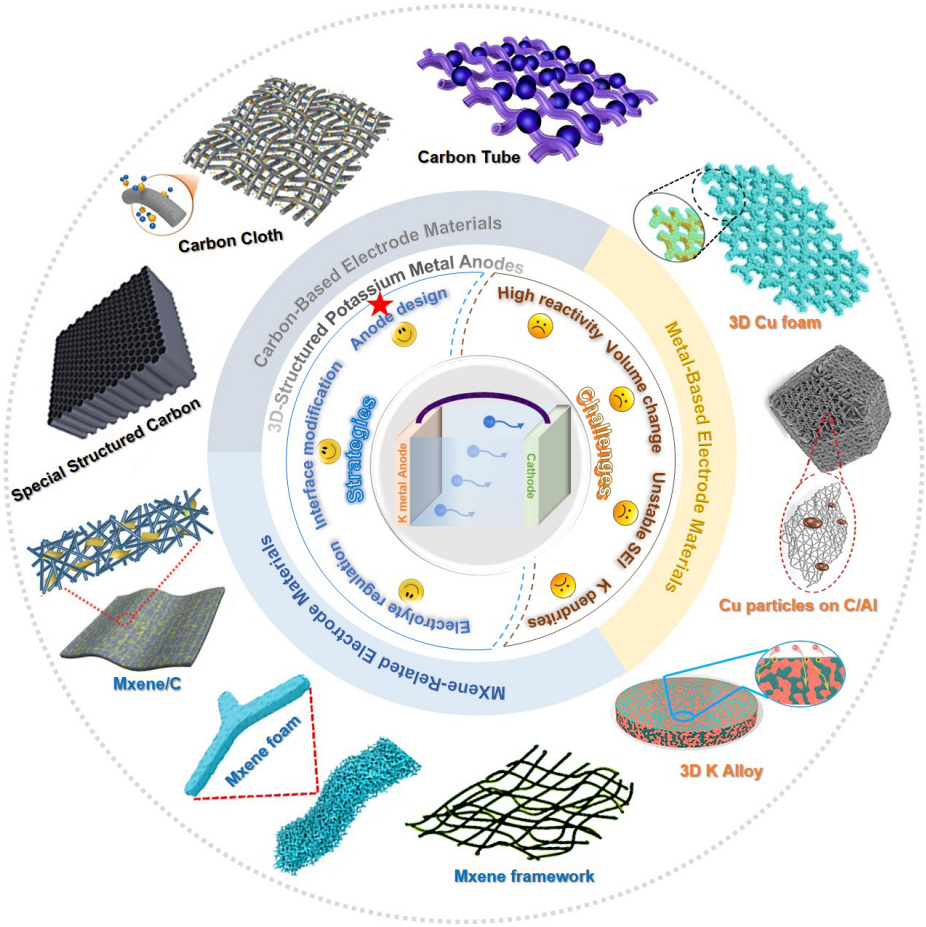

Figure 1. The challenges of potassium metal anodes and strategies to overcome them. The design of 3D-structured current collectors is taken as the effective strategy, including constructing carbon-based, metal-based, and MXene-related electrode materials.

full cell coupled with $K_{1.69}Fe[Fe(CN)_6]_{0.90}$ (PB) exhibited competitive cycling and rate performances, including a CE of 98.5% and a capacity of 84 mAh g^{-1} after 1,000 cycles at 0.5 C. The excellent electrochemical performance of K-ACM-based cells is beneficial because of their highly porous structure for K accommodation and local current density reduction, mechanical and structural stability to mitigate volume changes, and efficient electronic/ionic pathways to perform electrochemical redox reactions.

In addition to building a 3D host with a potassiophilic surface and infusing K into the 3D-K anode, the formation of a stable SEI layer is also an effective strategy. Ye *et al.* prepared N-doped C polyhedrons/graphene (HNCP/G) with metallic K plated inside (3D-K) and a solid electrolyte protective interface coating of Sn-based materials (Sn@3D-K)[68]. Figure 3A shows that the specific synthetic process mainly includes three steps: fabrication of HNCP/G with 0.1-2.1 μm HNCP particles anchored on the graphene surface; plating 5 mAh cm^{-2} K at 1.0 mA cm^{-2} into the HNCP/G to construct 3D-K; and preparation of the Sn-based SEI coated surface using the ion exchange method. The as-prepared Sn@3D-K has several advantages for K anode applications: Sn-based SEI to reduce side reactions and facilitate K ion transportation, formation of a KSn alloy to induce uniform nucleation and suppress dendrites, and a stable HNCP/G substrate to accommodate volume change and maintain structural integrity. Therefore, the Sn@3D-K cell exhibit long-term cyclic stability for 500 h at 0.2 mA cm^{-2} with low voltage polarization of 9 mV (100 h at 1.0 mA cm^{-2} with 31 mV). The full cell obtained using $K_{1.56}Mn[Fe(CN)_6]_{1.08}$/G as the cathode

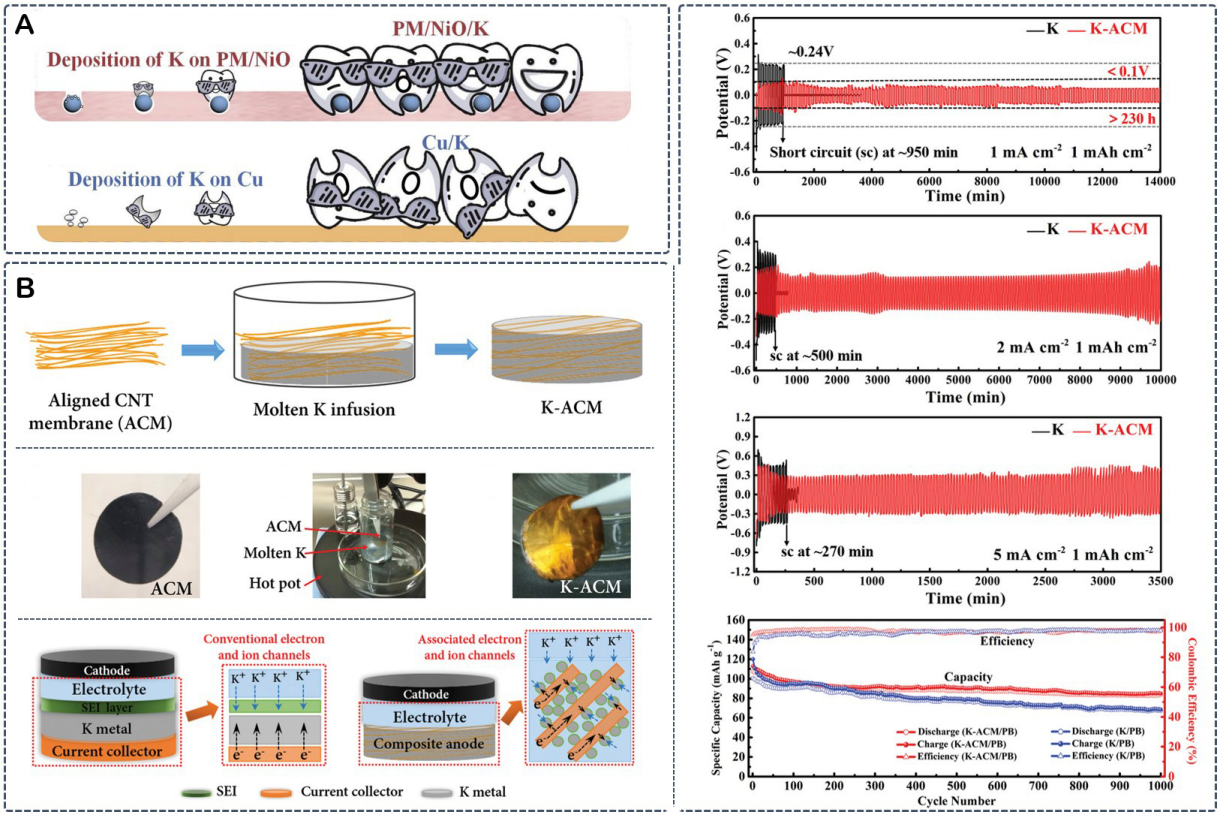

Figure 2. (A) Illustrations of the dendrite-free PM/NiO/K and caducous dendritic Cu/K electrode. This figure is quoted with permission from Li *et al.*[66]. (B) The fabrication process of the K-ACM, and schematics of electron and ion channels in a traditional chunk of metallic K and in a K-ACM electrode; electrochemical performance of symmetric cells with bare K or K-ACM electrodes; comparison of the cyclic stability and coulombic efficiency of the K-ACM/PB and K/PB cells at a rate of 0.5 C. This figure is quoted with permission from Qin *et al.*[67].

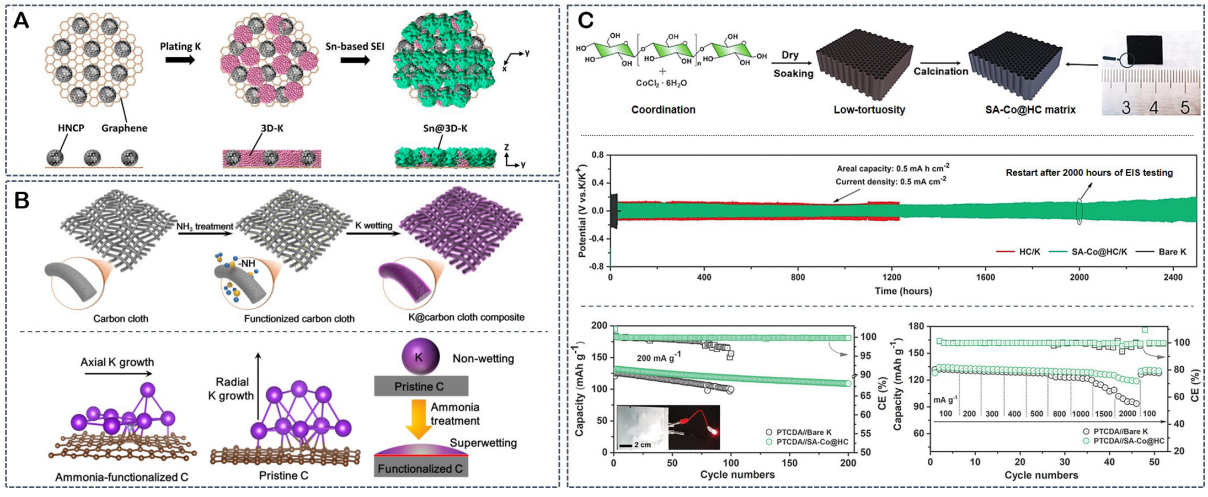

Figure 3. (A) Schematic of the preparation process for Sn@3D-K. This figure is quoted with permission from Ye *et al.*[68]. (B) The fabrication process of K wetting on active carbon cloth, DFT calculation of K growth on treated and untreated carbon surfaces, and the greatly improved wettability of the K metal on the functionalized carbon host. This figure is quoted with permission from Meng *et al.*[69]. (C) The synthesis of the SA-Co@HC; cycle stability of the symmetric cells at 0.5 mA cm^{-2} with a fixed areal capacity of 0.5 mAh cm^{-2}; cycling and rate performance of full cells with SA-C@HC/K and bare K anode and a PTCDA cathode at different current densities. This figure is quoted with permission from Zhang *et al.*[70].

exhibited an apparent diffusion coefficient of 4.55 × 10^{-6} cm^2 s^{-1} for K ions, which is 10^6 times that of the KMnHCF/G//K-foil cell. Therefore, when compared with the K foil or 3D-K-based full cells, the Sn@3D-K cell exhibits superior electrochemical performances, including close to the theoretical capacity value of 147.2 mAh g^{-1}, high average discharge plateau of 4.02 V, low overpotential of 0.01 V during cyclic stability tests, and improved rate capability.

As demonstrated by the above results, the introduction of a 3D host and "potassiophilic" surface is an attractive strategy for synthesizing K metal anodes. However, the method is usually correlated with complex 3D scaffolds or nonuniform distribution of the "potassiophilic" sites. Therefore, the rational design of lightweight carbon hosts with evenly distributed K-affinity sites is highly desired. Meng *et al*. prepared a carbon-based anode using a facile and effective method, that is, the functionalization of a carbon cloth (CC) surface with NH_3[69]. As illustrated in Figure 3B, the preparation process included the calcination of a CC to obtain the -NH surface and tune the wettability of the CC via NH_3 functionalization. The NH_3-funcationlized walls exhibit high wetting capability toward metallic K. According to DFT calculations, the ammonia-treated carbon host favored the 2D surface growth of K rather than the vertical growth style [Figure 3B]. Through the morphological evolution of the K@CC anode with cycling, a stable SEI was initially formed on the surface, promoting stable plating/stripping with cycling; the volume change could be accommodated by the 3D CC host. Therefore, the K@CC symmetric cell cycled at 1.0 mA cm^{-2} and 1.0 mA h cm^{-2} exhibited exceptional rate capability and stable cyclic performance for more than 180 cycles with low overpotentials of 240 mV; the $K_{0.7}Mn_{0.7}Ni_{0.3}O_2$|K@CC full cell also exhibited superior rate capability and cycling stability, that is, capacity of 114 mAh g^{-1} and capacity retention of 95% after 130 cycles at 0.1 A g^{-1}, and capacity of 55.5 mAh g^{-1} and retention of 68.5% even after 8,000 cycles at 1 A g^{-1}.

In the early stages of the electrode structural design for K metal anodes, Zhang *et al*. gained inspiration from natural wood with open, aligned, and stable channels to transport water to the entire tree[70]. They designed a low-tortuosity carbon host with an N-dopant and single-atom Co decoration, denoted as SA-Co@HC. The detailed preparation process is shown in Figure 3C, including the hydrothermal processing of the birch trunk in the $CoCl_2$-containing ethanol/hydrochloric acid solution, the strong coordination of Co with the polar functional groups containing oxygen, and heat treatment to form single Co atoms on the N-doped carbon (NC) support. The as-prepared SA-Co@HC matrix well-preserved the architecture of natural wood with orientated rough microchannels (5-50 μm diameter) and transverse pores. The Co atoms were highly dispersed, forming a Co-Nx-C coordination environment and increasing the number of active sites. Benefiting from the synthetic effect of single-atom chemistry and low-tortuosity host design, the as-prepared SA-Co@HC matrix has several distinctive advantages, such as straight aligned microchannels to alter the current density and ion pathways, enhanced affinity towards K with the dispersed Co atoms and N dopants, and sufficient space for K accommodation to suppress volume changes. During the deposition process, K ions transfer along the channels and deposit on the walls as nucleation sites, guiding the subsequent growth process. Therefore, the SA-Co@H/K symmetric cell exhibits long-term cyclic stability for over 2,500 h with low overpotentials of 130 mV at 0.5 mA cm^{-2} and 0.5 mAh cm^{-2}, which are significantly better than those of HC/K or bare K cells. This advanced single Co-atom-decorated HC host has wide generality and can be extended to other single metals, such as Fe and Ni, as demonstrated by the symmetric cell tests. The SA-Co@H/K-based full cell exhibited high cyclic and rate performances, that is, an initial capacity of 130 mAh g^{-1} and capacity retention of 84% after 200 cycles at 200 mA g^{-1}; a well-retained capacity of 122 mAh g^{-1} at 2,000 mA g^{-1}, which is superior to that of perylene-3, 4, 9, and 10-tetracarboxylic dianhydride//bare K full cells. Table 1 lists the host materials, synthetic methods, and electrochemical performances of the recently reported carbon-based K metal anodes.

Table 1. Details of the host materials, synthetic methods, and electrochemical performances of various carbon-based K metal anodes

Host	Surface/interface/active sites	K composite electrode	Electrolyte	Synthetic method	Symmetric cell rates; current density (mA cm^{-2}), capacity (mAh cm^{-2}), cycle life (h), and overpotentials (mV)	Half-cell performance (coulombic efficiency) current density (mA cm^{-2}), capacity (mAh cm^{-2}), cycle life (h), and CE (%)	Full cell cathode; rate; initial capacity, cycle life, and capacity retention	Refs
(Carbon-based material) PM/NiO	NiO	Electrodeposition	1.0 M KPF_6 in 1:1 v/v EC/DEC	Pore-forming reaction	0.1-1.6 mA cm^{-2}; 0.4 mA cm^{-2}, 200 cycles	0.4 mA cm^{-2}, 200 cycles, CEs 99.771%	PPB; 0.1-2 A; 0.1 A g^{-1}, 160 mAh g^{-1} after 180 cycles, 82% retention	[66]
Aligned carbon nanotube membrane (ACM)		Molten K infusion	0.8 M KPF_6 in EC/DEC, v/v = 1:1		1 mA cm^{-2}, 1 mAh cm^{-2}, 14,000 mins, 0.1 V; 2 mA cm^{-2}, 1 mAh cm^{-2}, 10,000 mins, 0.13 V; 5 mA cm^{-2}, 1 mAh cm^{-2}, 3,500 mins, 0.31 V		PB ($K_{1.69}Fe[Fe(CN)_6]_{0.90}$); 0.5 to 1, 2, 3, 4, and 5 C; 1,000 cycles@0.5 C, 84 mAh g^{-1}, and CE of 98.5%	[67]
Carbon nanotubes (CNTs)		Molten K infusion	1.0 M KFSI in EC/DEC (1:1 vol%)		0.5-6 mA cm^{-2}, 1 mAh cm^{-2}; 1 mA cm^{-2}, 1 mAh cm^{-2}, 500 h; 1 mA cm^{-2}, 2 mAh cm^{-2}, 600 h; 1 mA cm^{-2}, 3 mAh cm^{-2}, 500 h		Organic cathode PTCDA; 25-500 mA g^{-1}; 50 mA g^{-1}, 300 cycles, 124 mAh g^{-1}, and 86.7% retention	[71]
CoZn-embedded hollow carbon tubes (CoZn@HCT)	CoZn nanoparticles	K molten infusion	1.0 M KFSI in DME	Coaxial electrospinning and thermal annealing	0.5-5 mA cm^{-2}; 0.5 mA cm^{-2}, 0.5 mA h cm^{-2}, 1,100 h, 40 mV; 1 mA cm^{-2}, 1 mA h cm^{-2}, 1,000 h	1 mA cm^{-2}, 0.5 mA h cm^{-2}, 350 cycles, CEs 96.9%	Organic cathode (PTCDA); 0.02-1 A g^{-1}; 0.1 A g^{-1}, 200 cycles, 87 mA h g^{-1}, 71% retention	[72]
N-doped C polyhedrons/graphene (HNCP/G)	Sn-based SEI	Electrodeposition	KFSI in DME (mole ratio = 0.5)	Carbonizing ZIF-8/graphene composite; ion-exchange strategy	0.2 mA cm^{-2}, 1 mAh cm^{-2}, 500 h, 10 mV; 1 mA cm^{-2}, 1 mAh cm^{-2}, 100 h, 30 mV		$K_{1.56}Mn[Fe(CN)_6]_{1.08}$ /G(KMnHCF), 1.0 C, initial 108.2 mAh g^{-1}, 150 cycles, 73.5 mAh g^{-1}, CE 97.9%, and retention 67.9%	[68]
Atomic Co catalysts in N-doped carbon (SA-Co@HC)	Co-Nx-C	Molten K injection	3 M KFSI in EC/DEC (1:1, v:v)	Hydrothermal process and heating treatment	0.5-5.0 mA cm^{-2}, 0.5 mAh cm^{-2}; 0.5 mA cm^{-2}, 0.5 mAh cm^{-2}, 2,500 h, 130 mV; 1.0 mA cm^{-2}, 1.0 mAh cm^{-2}, 900 h, 100 mV		Organic cathode: PTCDA; 100-2,000 mA g^{-1}; 200 mA g^{-1}, initial 130 mAh g^{-1}, 200 cycles, retention 84%	[70]
Amine-functionalized	-NH site	Molten K	0.8 M KPF_6 in	Calcination activation	1-5 mA cm^{-2}, 1 mAh cm^{-2};		$K_{0.7}Mn_{0.7}Ni_{0.3}O_2$; 0.1-2.0 A g^{-1};	[69]

carbon cloth (CC)		infiltration	EC and DEC (1:1 in vol%)	and NH_3 functionalization	1 mA cm^{-2}, 1 mAh cm^{-2}, 180 cycles, 240 mV		0.1 A g^{-1}, 130 cycles, 114 mAh g^{-1}, 95% retention	
Ag on carbon cloth (Ag-CC)	Ag nanoparticles	Electrodeposition	0.8 M KPF_6 in 1:1 (vol%) EC and DEC	Solution soaking and calcination	0.5 mA cm^{-2}, 0.5 mA h cm^{-2}, 700 h, 41 mV		Potassium Prussian blue (PPB); 0.5-5.0 C; 1 C, 600 cycles, > 70 mAh g^{-1}	[73]
Co-embedded nitrogen-doped carbon nanofiber paper (Co-CNFs)	Co nanoparticles and N doping	Molten K infusion	1.0 M KFSI in DME	Electrospinning and carbonization	0.5 mA cm^{-2}, 0.5 mAh cm^{-2}, 1,300 h, 50 mV; 2 mA cm^{-2}, 1 mAh cm^{-2}, 500 h	1 mA cm^{-2}, 1 mAh cm^{-2}, 400 cycles, CEs 98.75%; 2 mA cm^{-2}, 4 mAh cm^{-2}, 120 cycles, CEs 98.74%	Organic cathode AQDS; 1-15 C, 5C, 700 cycles, retention 58%	[74]
Oxygen-rich treated carbon cloth (TCC)	Oxygen functional groups		1.0 M KFSI-DME		5.0 mA cm^{-2}, 5.0 mAh cm^{-2}, 1,400 h, 60 mV	1 mA cm^{-2}, 1 mAh cm^{-2}, 1,000 cycles, CEs 99%; 3 mA cm^{-2}, 3 mAh cm^{-2}, 800 cycles, CEs 99.4%		[75]
Carbon nanofiber paper (CBC)	Oxygen- functional groups	K melt-infusion	1.0 M KFSI-DME; 3.0 M KFSI-DME	Carbonizing bacterial cellulose (BC)	0.5 mA cm^{-2}, 0.5 mAh cm^{-2}, 1,400 h, 45 mV;1 mA cm^{-2}, 1 mAh cm^{-2}, 1,200 h, 55 mV	1 mA cm^{-2}, 1 mAh cm^{-2}, 350 cycles, CEs 98%	$K_4Fe(CN)_6$ (KFC); 10-100 mA g^{-1}; 20 mA g^{-1}, 500 cycles, 85% retention	[76]
SnO_2-modified carbon cloth (CC@SnO_2)	SnO_2 nanoparticles	K molten infusion	1 M KFSI in EC and DEC (1:1 vol%)	Solvothermal and calcination treatment	0.5-5.0 mA cm^{-2}, 1 mAh cm^{-2}; 0.5 mA cm^{-2}, 1 mAh cm^{-2}, 635 h, 150 mV; 1 mA cm^{-2}, 1 mAh cm^{-2}, 380 h, 170 mV		PTCDI;50-5,000 mA g^{-1}; 500 mA g^{-1}, 6,000 cycles, 84 mA h g^{-1}; 2 A g^{-1}, 10,000 cycles, 70.9% retention	[77]
SnO_2-coated carbon nanofiber (PCNF@SnO_2)	SnO_2 coating layer	K molten infusion	1.0 M KFSI-DME	Electrospinning, carbonization, and atomic layer deposition	0.5-6 mA cm^{-2}; 0.5 mA cm^{-2}, 0.5 mA h cm^{-2}, 1,700 h, 50 mV; 1 mA cm^{-2}, 1 mA h cm^{-2}, 1,700 h	1 mA cm^{-2}, 1 mA h cm^{-2}, 150 cycles, average CEs 98.3%	Organic cathode: AQDS; 1-25 C; 5C, 400 cycles, 75% retention	[78]
CuO on carbon fiber cloth (CC@CuO)	CuO nanoparticles	Molten K infiltrate	1M KFSI in EC/DEC (1:1 by vol%)	Hydrothermal and thermal treatments	0.5-6 mA cm^{-2}; 0.5 mA cm^{-2}, 0.5 mA h cm^{-2}, 1,200 h; 0.5 mA cm^{-2}, 1 mA h cm^{-2}, 800 h; 0.5 mA cm^{-2}, 2 mA h cm^{-2}, 2,000 h		PTCDA/rGO; 10-200 mA g^{-1}; 20 mA g^{-1}, 200 cycles, retention 53.2%; $K_{0.5}V_2O_5$ (KVO); 25-500 mA g^{-1}; 50 mA g^{-1}, 500 cycles, retention 80%	[79]
SnS_2 nanosheets loaded on carbon paper (SnS_2@CP)	SnS_2 nanosheets	Electrodeposition	1 M KPF_6 in (EC/DEC) (vol% 1:1)	HNO_3 soaking and heat treatment	0.25 mA cm^{-2}, 0.25 mAh cm^{-2}, 800 h, 70 mV; 1 mA cm^{-2}, 1 mAh cm^{-2}, 260 h	0.25 mA cm^{-2}, 0.25 mAh cm^{-2}, 150 cycles, CEs > 95%	Potassium Prussian blue (KPB), 0.05-0.2 A g^{-1}; 0.05 A g^{-1}, initial 65.6 mAh g^{-1}, 150 cycles, retention 86.9%; 0.1 A g^{-1}, initial 60.6 mAh g^{-1}, 200 cycles, retention 83.7%	[80]

METAL-BASED ELECTRODE MATERIALS

Cu-based electrode materials

Metal-based current collector matrices with excellent mechanical properties and stability have been widely applied in Li or Na metal anodes. Yang *et al*. first applied a 3D porous Cu skeleton as a current collector to optimize the lithium deposition behavior, which was highly improved compared with the conventional 2D Cu[81]. Appropriate pore size, volume, and distribution are important for high-performance Li metal anodes. A large pore structure has a limited surface area for even deposition regulation; pores that are too small may limit lithium-ion diffusion and volume changes. Therefore, a high-performance 3D current collector requires the rational design of porous structures. Cu-based 3D current collectors for Li metal anodes have been extensively investigated and reviewed[54]. Based on their pore structures, 3D Cu current collectors can be divided into three categories. The first type is a disordered pore structure, which is easier for scalable production, even though the pore structure is difficult to control. For example, Yun *et al*. modulated the pore size through a simple chemical dealloying method of Cu-Zr alloys and tuned the treatment time[82]. The second type is an ordered pore structure, such as a 3D mesh prepared using a facile one-pot method[83]. The third type is related to special pore structures, including elastic pores for stress relaxation[84], gradient pores to improve space utilization[85], and the bidirectional pore structure desired for practical applications[86]. Additionally, because the Li nucleation energy on Cu remains very large, a lithiophilic surface design on the 3D Cu skeleton is commonly applied, including metal-forming alloys with Li, metal compounds as conversion reaction materials with Li, and heteroatom-doped carbon materials[54]. For Na metal anodes, Wang *et al*. fabricated a copper nanowire-reinforced 3D Cu foam as a current collector to increase the number of nucleation sites and decrease the local current density for uniform Na deposition[87,88]. The electrochemical performance of a 3D Cu Na current collector can be improved by modifying its sodiophilic surface with oxides and sulfides[89,90]. Moreover, the performance can be further enhanced by the protective layer over the "sodiophilic" surface to suppress side reactions[91].

To achieve stable K plating/stripping, Liu *et al*. utilized the synergistic effect of a 3D geometric Cu current collector combined with the potassiophilic surface chemistry effect of a reduced graphene oxide (rGO) coating, denoted as rGO@3D-Cu[92]. Specifically, the rGO@3D-Cu was fabricated using a combination of self-assembly and partial reduction strategies. As shown in Figure 4A, the graphene oxide (GO) layers are reduced, and the rGO layers stack on the surface of the 3D-Cu foam. The as-prepared rGO@3D-Cu exhibited highly enhanced potassiophilicity compared to the 3D-Cu foam, according to the K wetting behavior test. Moreover, the rGO@3D-Cu-based symmetric cells and half-cells exhibited superior electrochemical performance compared to 3D-Cu or planar (rGO)@Cu. During the symmetric cell tests, the rGO@3D-Cu cell cycled stably over a wide current density range of 0.1-2.0 mA cm^{-2}, in contrast to the fading of Cu cell at a low current density of 0.5 mA cm^{-2}. Upon measurement of the half-cell, it was demonstrated that the rGO@3D-Cu cell exhibits cyclic stability for 10,000 mins at 0.5 mA cm^{-2} and 5,000 mins at 1.0 mA cm^{-2}, in contrast to the early fading after 5,110, 3,012, and 1,410 mins of the 3D-Cu, planar rGO@Cu, and planar Cu, respectively. The excellent electrochemical performance of rGO@3D-Cu was beneficial owing to its synergistic chemical and geometrical effects. In comparison with 3D-Cu foam without surface rGO, the rGO surface exhibits higher surface tension compared to Cu, improving the K wettability and potassiophilicity; in contrast to rGO@Cu, the rGO@3D-Cu has a significantly larger surface area to reduce the effective current density and suppress dendrites initiation.

In addition to the rGO surface coating, Wang *et al.* fabricated a Cu_3Pt-functionalized 3D Cu mesh as a current collector for K anode applications[93]. As shown in Figure 4B, the Cu_3Pt-Cu electrode is prepared via the simple galvanic replacement reaction as follows: immerse the Cu mesh in the $[PtCl_6]^{2-}$ solution, deposit Pt on the Cu mesh surface with the dissolution of Cu atoms, and form Cu-Pt bimetallic alloy covered by rough Cu mesh. The Cu_3P exhibited high affinity toward K, as demonstrated by the DFT calculation of the

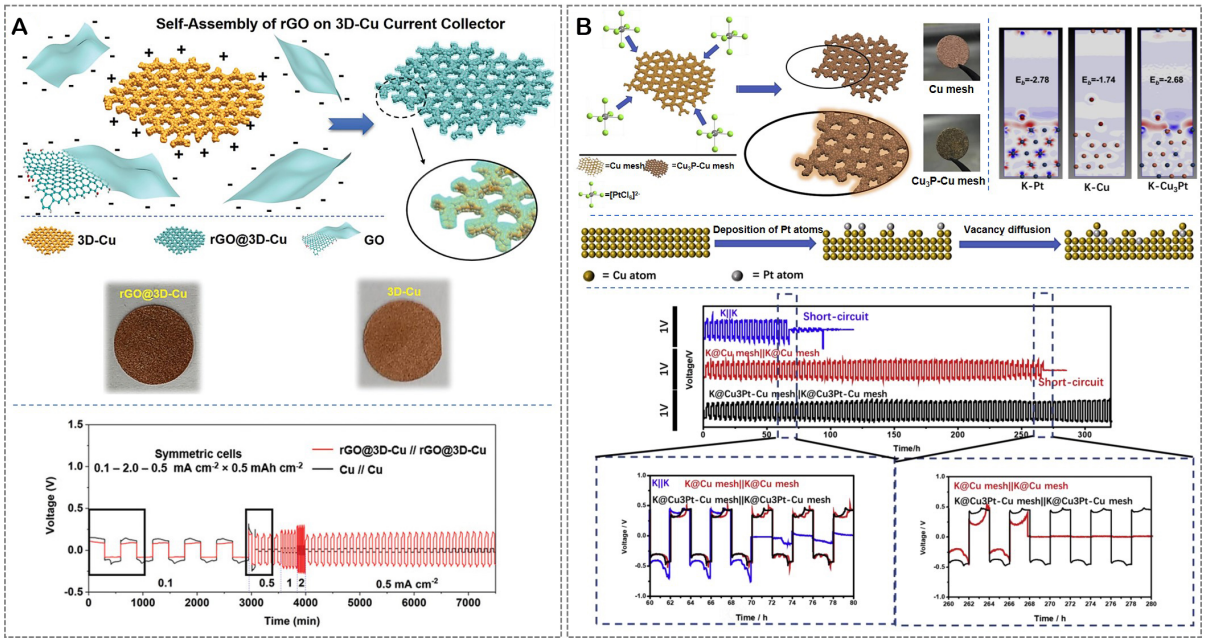

Figure 4. (A) The partially reduced graphene oxide (rGO) coated on a 3D-Cu current collector, termed rGO@3D-Cu; Thermally infused symmetric rGO@3D-Cu//rGO@3D-Cu, with baseline Cu//Cu. This figure is quoted with permission from Liu *et al.*[92]. (B) The fabrication of Cu_3Pt-Cu mesh, the process of Galvanic replacement reaction and the 2D electron density difference maps of K adsorbed Pt, Cu, and Cu_3Pt; Voltage-time profiles of K||K, K@Cu mesh||K@Cu mesh and K@Cu_3Pt-Cu mesh||K@Cu_3Pt-Cu mesh symmetric cells at 0.5 mA cm^{-2} and 1 mAh cm^{-2}. This figure is quoted with permission from Wang *et al.*[93].

binding energy of K with Pt (-2.78 eV), Cu (-1.74 eV), and Cu_3Pt (-2.68 eV). In combination with the facilitated electron transport pathways and ultrahigh surface area provided by the 3D Cu mesh, the as-prepared Cu_3Pt-Cu mesh current collector exhibited excellent electrochemical performance. The Cu_3Pt-Cu-based half-cell exhibited a long cycle life of 300 h with high CEs of 95% at 0.5 mA cm^{-2}. Its symmetric cell can maintain a stable voltage for more than 300 h with voltage hysteresis of 1,000 mV at 0.5 mA cm^{-2} and 1.0 mAh cm^{-2}; when increased to an ultra-high capacity of 5 mAh cm^{-2}, the K@Cu_3Pt-Cu symmetric cell is cyclable even for over 170 h. When coupled with a Prussian blue (KPB) cathode in a full cell, it can cycle for 270 cycles with 50 mAh g^{-1} maintained.

Wang *et al.* designed another K anode current collector using a Pd-coated Cu foam via a replacement reaction, denoted as K/Pd/Cu foam[94]. In accordance with their previous study[93], Pd and Pt, which belong to the same platinum group, exhibit similar properties. Pd exhibited higher affinity toward K, as demonstrated by the DFT calculations, as the binding energies between K and Cu (111) and Pd (111) were -2.70 and -3.11 eV, respectively [Figure 5A]. The deposited K atoms preferentially bonded with Pd and formed a Pd-K alloy as K nucleation sites to guide uniform deposition. In addition, the Pd/Cu foam increased the stability of the SEI and reduced the number of side reactions. Therefore, for the half-cell test of CEs with lithium deposition capacity ranging from 0.5 to 10 mA cm^{-2}, the Pd/Cu foam-based cell outperforms the Cu-based cell. Similarly, the Pd/Cu foam-based symmetric cells exhibit a longer cycle life span with more stable overpotentials over the wide deposition capacities of 1.0-10 mAh cm^{-2}. For the full-cell test, the K/Pd/Cu||PB cell exhibits a capacity of up to 58 mAh g^{-1} and a high CE of 96% after 100 cycles. More interestingly, the symmetric cell of K/Pd/Cu is cyclable at a low temperature of -20 °C for 3,400 min with a polarization potential of 2,000 mV; the K/Pd/Cu full cell exhibits a capacity of 38 $mAhg^{-1}$ with capacity retention of 97% after 60 cycles at 1.0 C.

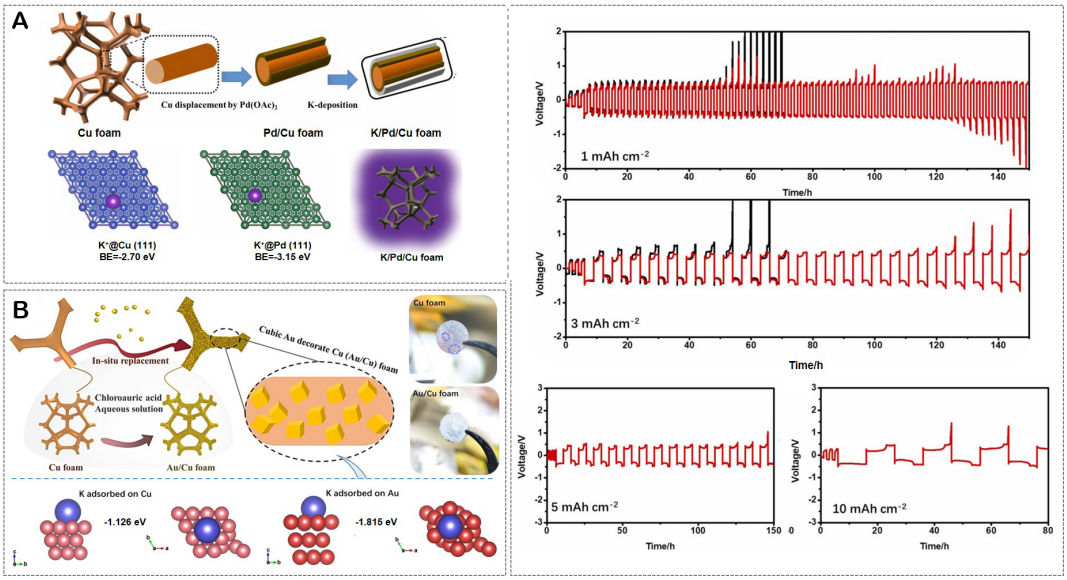

Figure 5. (A) The preparation of the Pd/Cu, K/Pd/Cu foam anodes, and the deformation charge density of K^+ absorbed on Cu and Pd substrates, respectively; Galvanostatic profiles for KMB cells with 1.0, 3.0, 5.0, and 10.0 mA h cm^{-2} of K on K/Pd/Cu foam and K/Cu foam. This figure is quoted with permission from Wang *et al.*[94]. (B) The synthesis and mechanism of Au/Cu foam current collector and the calculated adsorption energy of K^+ with Au and Cu. This figure is quoted with permission from Li *et al.*[95].

In addition to Pt and Pd, Li *et al.* decorated the platinum-group element Au[95] via a chemical replacement reaction on Cu foam for K anode applications. As shown in Figure 5B, the cubic Au nanoparticles were uniformly distributed on the Cu foam surface. Au atoms with a higher potassiophilicity than Pt are helpful for establishing a uniform electric field, guiding uniform ion diffusion across the SEI, and improving the mechanical properties of the interface. When assembled into cells, the as-prepared highly porous Au/Cu current collector exhibits several advantages, including decreasing the local current density, promoting uniform nucleation, stabilizing the interface, suppressing side reactions, and restricting volume expansion during cycling. As expected, the Au/Cu-based half/symmetric/full cells exhibit significantly better performance than the cells without Au coating both at room temperature and low temperature of -20 °C. A comparison of the host materials, synthetic methods, and electrochemical performances of various Cu-based current collectors is summarized in Table 2.

Other metal (Alloy)-based electrode materials

Commonly used current collectors for LIBs are Cu and Al foils. However, they are not applicable to lithium-metal batteries because of the reaction between Li and Al. For the K metal anode, there was no thermodynamic reactivity between K and Al. In comparison with the Cu foil, the Al foil exhibits several competitive features, including being four times cheaper than Cu and having only one-third the density of Cu. Liu *et al.* applied an Al-based current collector to K metal anodes for the first time[97]. As illustrated in Figure 6A, they designed an Al powder (mean diameter of 12 μm)-based 3D Al architecture layer with a thickness of 22 μm sintered on the Al foil, denoted as Al@Al. Additional samples of "Al@Al-D" (powder diameter of 3 μm, thickness of 22 μm) and Al foil were prepared for comparison. The Al@Al, Al@Al-D, and Al foils exhibited geometrical roughness values ranging from high to low, which corresponded to their electrolyte wetting behaviors. The electrochemical tests demonstrated that the Al@Al half-cell is cyclable for more than 1,000 cycles with high CEs of 98.9% at 0.5 mA cm^{-2}, and the K-Al@Al cell can cycle stably over the wide current density range of 0.1-3.0 mA cm^{-2}, which are significantly better than those of Al@Al-D and Al foil-based cells. The authors correlated the electrochemical performance with the electrolyte wetting properties; that is, the poorer the electrolyte wetting, the earlier the occurrence of unstable SEI and dendritic initiation, and the easier the formation of K islands and dead K upon repeated plating/stripping.

Table 2. Details of the host materials, synthetic methods, and electrochemical performances of various Cu, Al, alloy, and Mxene-based K metal anodes

Host	Surface /interface /active sites	K composite electrode	Electrolyte	Synthetic method	Symmetric cell rates; current density (mA cm^{-2}), capacity (mAh cm^{-2}), cycle life (h), and overpotentials (mV)	Half-cell performance (coulombic efficiency) current density (mA cm^{-2}), capacity (mAh cm^{-2}), cycle life (cycles), and CE (%)	Full cell cathode; rate; initial capacity, cycle life (cycles), and capacity retention (%)	Refs
Reduced graphene oxide on 3D-Cu (rGO@3D-Cu)	Structural defects and O/OH groups	K molten infusion	0.8 M KPF_6 in EC/DEC/PC (2:1:2 vol%)	Self-assembly and partial reduction	0.1-2.0 mA cm^{-2}, 0.5 mAh cm^{-2}; 0.5 mA cm^{-2}, 0.5 mAh cm^{-2}, 200 h, ~200 mV	0.5 mA cm^{-2}, 0.5 mAh cm^{-2}, 100 cycles		[92]
Cu_3Pt-functionalized Cu mesh (Cu_3Pt-Cu)	Cu_3Pt	Press K with the punching machine	1 M KPF_6 in 1:1 (v/v) EC/DEC + FEC	Galvanic replacement reaction	0.5 mA cm^{-2}, 1 or 2 or 3 mAh cm^{-2}, 300 h, 500 mV; 5 mAh cm^{-2}, 170 h	0.5 mA cm^{-2}, 0.5 mAh cm^{-2}, 300 cycles, CEs > 95%	Prussian blue (KPB), 200 cycles, 51 mAh g^{-1}, 71.8% retention	[93]
Pd-coated Cu foam (Pd/Cu)	Pd-(K alloy)	K deposition	3 M KFSI-DME	Replacement reaction	1.0 mAh cm^{-2}, 130 h; 3.0 mAh cm^{-2}, 500 mV; 5.0 and 10 mAh cm^{-2}	0.5 mA cm^{-2}, 0.5 mAh cm^{-2}, 450 cycles; 0.5 mA cm^{-2}, 1 mA h cm^{-2}, > 400 cycles, CEs 98.0%; 5 and 10 mA h cm^{-2}, CEs ~100%	Prussian blue (PB), 100 cycles, 58 mA h g^{-1}, and CEs 96%	[94]
Gold-decorated 3D copper foam (Au/Cu foam)	Au particles	K deposition	3 M KFSI in DME; 0.8 M KPF_6 in EC:DEC (1:1) + 5 vol% FEC	Chemical replacement reaction	1 mA cm^{-2}, 1 mAh cm^{-2}, 350 h, 500 mV; 5 and 10 mAh cm^{-2}, 180 h	1 mA cm^{-2}, 1 mAh cm^{-2}, 500 cycles	Prussian blue (KPB), 0.5 A g^{-1}, 350 cycles, 64 mAh g^{-1}, and CEs 98%	[95]
Cu_2Se-modified 3D copper framework (K_2Se/Cu)	K_2Se	K thermal infusion	1.0 M KFSI in EC:DEC = 1:1	Solution selenization	0.5-5 mA cm^{-2}; 0.5 mA cm^{-2}, 0.5 mAh cm^{-2}, 1,000 h, 180 mV			[96]
Aluminum-powder-coated aluminum foil (Al@Al)	Al powders	Pre-potassiated	4 M KFSI in DME	Sintering		0.1-3.0 mA cm^{-2}, 0.5 mAh cm^{-2}; 0.5 mA cm^{-2}, 0.5 mAh cm^{-2}, 440 h; 3.0 mA cm^{-2}, 0.5 mAh cm^{-2}, 2,600 min		[97]
Nitrogen-doped carbon@graphdiyne-modified Al current collector (NC@GDY-Al)	Cu QD on NC@GDY	K electrodeposition	4M KFSI-DME	Copper envelope method	0.4-5.0 mA cm^{-2}, 1 mAh cm^{-2}; 0.5 mA cm^{-2}, 0.5 mAh cm^{-2}, 2,400 h, 10 mV; 2 mA cm^{-2}, 2 mAh cm^{-2}, 2,400 h, 20 mV; 2 mA cm^{-2}, 4 mAh cm^{-2}, 800 h, 50 mV	0.2-5.0 mA cm^{-2}; 0.2 mA cm^{-2}, 0.2 mAh cm^{-2}, 800 cycles, CEs 99.93%	$K_{0.220}Fe[Fe(CN)_6]_{0.805}\cdot 4.01H_2O$ (KPB); 20-2,000 mA g^{-1}	[98]
3D-K_3Bi@K	K_3Bi matrix	Molten K reaction	1.0 M KFSI in EC/DEC = 1:1 vol%	High-temperature reaction	0.5 mA cm^{-2}, 1 mAh cm^{-2}, 450 h			[99]

3D alkalized Ti_3C_2 MXene nanoribbon (α-Ti_3C_2)	F-/O-terminated functional groups	Electrodeposition	0.8 M KFSI in EC:DEC (1:1, v/v)	HF etching and alkalization	3 mA cm^{-2}, 3 mAh cm^{-2}, 100 h, 14 mV; 5 mA cm^{-2}, 5 mAh cm^{-2}, 800 h, 18 mV; 5 mA cm^{-2}, 10 mAh cm^{-2}, 700 h, 11 mV	1.0 mA cm^{-2}, 1.0 mAh cm^{-2}, 300 cycles, CEs 99.5%; 3.0 mA cm^{-2}, 3.0 mAh cm^{-2}, 300 cycles, CEs 99.4%	$K_2Ti_4O_9$ (KTO); 50-500 mA g^{-1}; 200 mA g^{-1}, 97.5 mA h g^{-1}, 1,000 cycles	[100]
3D Ti_3C_2TX MXene-melamine foam (MXene-MF)	F-/O-terminated groups	K pre-deposition	0.8 M KFSI in EC and DEC	MXene ink soaking	1-7 mA cm^{-2}; 5 mA cm^{-2}, 5 mAh cm^{-2}, 800 h	5 mA cm^{-2}, 5 mAh cm^{-2}, 55 cycles, CEs 96%		[101]
Defect-rich and nitrogen-containing MXene (DN-MXene)	-OH, =O, and -F	K melt infusion	0.8 M KPF_6/KFSI in EC:DEC (1:1, v/v)	Etching & Sonication and mix & filtration	0.1-2 mA cm^{-2}; 0.5 mA cm^{-2}, 300 h, 300 mV	0.5 mA cm^{-2}, 5 mA h cm^{-2}, 200 cycles, CEs 98.6%	Sulfur; 0.1-5.0 C; 0.5 C, 31 mAh g^{-1}, 500 cycles, 230 mA h g^{-1}	[102]

Following the report by Liu *et al.*, Yi *et al.* modified the surface of an Al current collector with potassiophilic graphdiyne (GDY) for K anode applications[98]. As shown in Figure 6B, the synthetic procedure included the synthesis of NC as a growth template for GDY and the growth of GDY with attached Cu quantum dots (QDs) on the NC template using the copper enveloping method. The as-prepared NC@GDY-Al electrode exhibits significant structural and chemical advantages: (1) the NC template can improve the conductivity and specific surface area of the electrode; (2) GDY is able to provide sufficient K^+ ion transportation pathways and K nucleation sites; and (3) the interspersed Cu QDs further increases the affinity towards K and the overall electrical conductivity. Therefore, compared with the Al-, NC-Al- or NC@GDY-Al- (without Cu)-based cells, the NC@GDY-Al(Cu) asymmetric cell exhibits smaller nucleation overpotential, stable K plating/stripping for more than 2,000 h, remarkably high CE of 99.93% for over 800 cycles, and impressive rate capability over the wide current density range of 0.2-5.0 mA cm^{-2}. The NC@GDY symmetric cells tested at 0.5/0.5, 2.0/2.0, and 2/4 (mA cm^{-2}/mAh cm^{-2}) can cycle stably for over 2,000, 2,400, and 850 h with low overpotentials of 10, 20, and 50 mV, respectively. The cyclic stability and low voltage hysteresis of the NC@GDY symmetric cells are manifested from 0.4 to 5.0 mA cm^{-2} with a fixed capacity of 1.0 mAh cm^{-2}. The full cell assembled using the KPB ($K_{0.220}Fe[Fe(CN)_6]_{0.805}\cdot 4.01H_2O$) cathode and the NC@GDY anode also exhibited superior cycling and rate performances.

According to previously reported 3D current collectors, a desired 3D host should exhibit both high ionic and electronic conductivities, resulting in uniform K deposition and suppressing dendrites growth. Ye *et al.* prepared a 3D-K_3Bi@K electrode via high-temperature treatment of K metal and Bi powder, followed by rolling and cutting it into disks after cooling down[99]. The as-prepared 3D K_3Bi framework exhibited high electron/ionic conductivities and potassiophilic properties, providing various advantages for K anode applications, including homogeneous and heterogeneous nucleation, buffered volume expansion, and suppressed side reactions with the electrolyte [Figure 6C]. Therefore, the 3D-K_3Bi@K electrode exhibits long-term cyclic stability for 450 h at 0.5 mA cm^{-2} at a fixed capacity of 1.0 mAh cm^{-2}, in contrast to the early short-circuit of the K anode after merely 56 h.

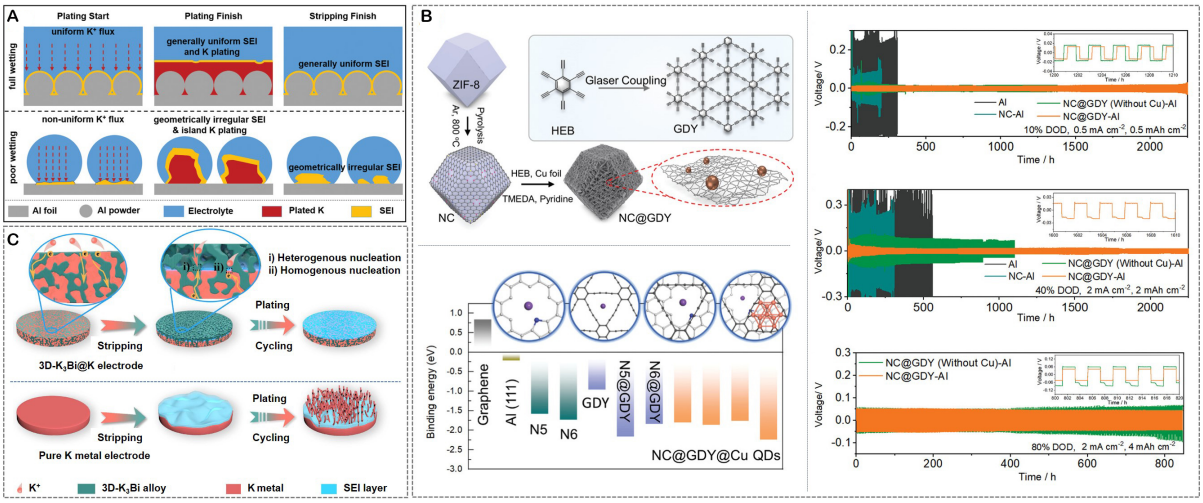

Figure 6. (A) Electrolyte wetting on Al@Al and Al foil and their corresponding effect on the plating/stripping behaviors. This figure is quoted with permission from Liu *et al.*[97]. (B) Schematic illustrating the synthetic steps of NC@GDY and the potassium adsorption energy on various substrates; cyclic stabilities of symmetric cells with different electrodes at 0.5 mA cm^{-2}/0.5 mAh cm^{-2}, 2.0 mA cm^{-2}/2.0 mAh cm^{-2}, and 2.0 mA cm^{-2}/4.0 mAh cm^{-2}. This figure is quoted with permission from Yi *et al.*[98]. (C) Comparison of the K plating/stripping processes on 3D-K_3Bi@K and pure K metal electrodes. This figure is quoted with permission from Ye *et al.*[99].

MXENE-RELATED ELECTRODE MATERIALS

MXene ($Ti_3C_2T_x$) has been widely applied in Li or Na metal anodes because of its several advantages, including high electronic conductivity, high ion diffusion capability, and strong affinity to alkali metals[103,104]. Delaminated MXene is prone to aggregation, which reduces the number of alkali deposition sites and the electrochemical performance. Therefore, the rational design of a 3D MXene network with a large surface area and sufficient potassiophilic sites is important for its application in K metal anodes.

Shi *et al.* prepared a 3D alkalized Ti_3C_2 (α-Ti_3C_2) MXene nanoribbon host for K metal anodes[100]. As illustrated in Figure 7A, the specific synthesis procedure included the preparation of a densely stacked Ti_3AlC_2 MAX precursor, etching of the Al atom in an acidic solution (m-Ti_3C_2), delamination of m-Ti_3C_2 into 2D d-Ti_3C_2, and shaking m-Ti_3C_2 in KOH to obtain a 3D α-Ti_3C_2 framework. The as-prepared 3D host with a wide-open porous structure had a large surface area to reduce the local current density and an efficient electronic/ionic transportation network. In addition, F- and O- functional groups with highly potassiophilic characteristics were evenly distributed over the 3D surface to ensure uniform nucleation. Therefore, the α-Ti_3C_2-based cells exhibited excellent electrochemical performances: the CEs were as high as 99.4% after 300 cycles at a current density of 3.0 mAh cm^{-2} and capacity of 3.0 mAh cm^{-2}. The symmetric cell exhibited ultra-high cyclic stability for 700 h with a small voltage polarization of 11 mV at an ultra-high current density of 5.0 mA cm^{-2} and capacity of 10 mAh cm^{-2}. The full cell coupled with $K_2Ti_4O_9$ (KTO) cathode also exhibited highly improved rate capability and cyclic stability compared with the pure K cell.

In addition to the direct design of 3D MXene scaffolds, the construction of MXene surfaces combined with 3D networks is also a reasonable strategy. Shi *et al.* fabricated 3D $Ti_3C_2T_X$ MXene-melamine foam (denoted as MXene-MF) using an effective and scalable method, and the as-prepared 3D scaffold was applicable to a wide range of high-performance alkali metal anodes, including Li, Na, and K[101]. As shown in Figure 7B, the 3D MXene-MF scaffold was fabricated by soaking highly porous MF in a concentrated MXene solution that was subsequently freeze-dried. During the drying process, adhesive hydrogen bonds are formed between the molecular chains of MF (NH_2, NH, and imine) and the surface functional groups of MXene (-OH and -F).

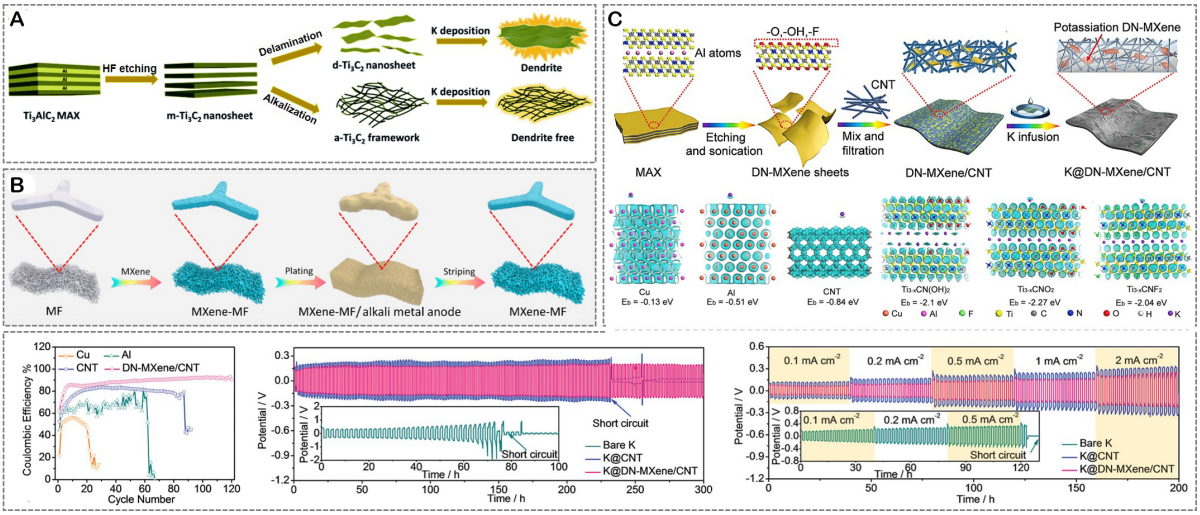

Figure 7. (A) Schematic illustration of the α-Ti_3C_2 Mxene nanoribbon framework and d-Ti_3C_2 Mxene nanosheet. This figure is quoted with permission from Shi *et al.*[100]. (B) Scheme of the fabrication process of the 3D Mxene-MF for the alkali-metal anode. This figure is quoted with permission from Shi *et al.*[101]. (C) Illustration for the preparation of the DN-Mxene/CNT scaffold and K@DN-Mxene/CNT metallic anodes; the Coulombic efficiencies of K plating/stripping on different scaffolds at 0.5 mA cm^{-2} in KPF_6-based electrolyte; voltage profiles of symmetric cells with K@DN-Mxene/CNT, K@CNT, or bare K metal anodes at 0.5 mA cm^{-2}; rate performances of three symmetric cells at different current densities. This figure is quoted with permission from Tang *et al.*[102]

Therefore, the MXene surface with high electronic conductivity and alkali affinity can facilitate charge transportation and homogenize the ionic flux, and in combination with the 3D MF with an interconnected porous network and high mechanical toughness, it further ensures low local current density and suppresses volume fluctuation. Consequently, the MXene-MF scaffold achieved superior electrochemical performance for the Li, Na, and K anodes. Notably, the MXene-MF-K symmetric cell achieves cyclic stability for 800 h at a current density of 5.0 mA cm^{-2} and capacity of 5.0 mAh cm^{-2}.

Tang *et al.* first introduced N-containing MXenes with rich defects for K metal anode applications[102]. As shown in Figure 7C, the K metal anode is prepared via the extraction of Al from the Ti_3AlCN-MXene precursor, a mixture of the obtained DN-MXene with CNTs (denoted as DN-MXene($Ti_{3-x}CNT_y$)/CNT), and infusion of K into the pores as the final composite electrode K@DN-MXene/CNT. The as-prepared 3D DN-MXene/CNT matrix with an interconnected porous architecture can provide efficient electron and ion transport pathways, accommodation space for the deposited K and volume change, and decreased local current density for uniform ionic flux. More importantly, the DFT results verified the high K-philic property of the $Ti_{3-x}CNT_y$ MXene based on the binding energy calculation, which can seed uniform K nucleation [Figure 7C]. As expected, the CEs of the DN-MXene/CNT-based two-electrode cell were as high as 93.1%, and small voltage gaps were observed during the 120 cycles; for the symmetric cell galvanostatic test, the K@DN-MXene/CNT cells exhibited both high cycling stability for 300 h with low voltage hysteresis of 0.3 V and superior rate capability; when assembled for full cell operation, the K@DN-Mxene/CNT// sulfur-poly(acrylonitrile) full cell with effective polysulfides suppression effect delivered high capacity and cyclic performance, all of which were significantly better than the results of bare K or (K@)CNT cells.

CONCLUSION AND OUTLOOK

This paper summarizes the recent progress of 3D-structured electrodes for K metal anode applications. The rational design of nanostructured anodes increased the effective surface area and provided sufficient K metal accommodation space without any significant volume fluctuations. Synergistically, the surface

potassiophilic sites decreased the nucleation barrier and guided the uniform deposition process, thereby improving the reversible K plating/stripping behavior and CEs values. This paper outlines advanced 3D structured hosts of K metal anodes based on the materials used, including carbon-based, metal-based, and MXene-related electrode materials. These three types of electrode materials exhibit unique characteristics and (dis)advantages in alkali-metal anode applications.

1. Carbon-based materials exhibit advanced characteristics that are beneficial for the application of alkali metal anodes, including low density, low cost, high electronic conductivity, high surface area, versatile structures, and fabrication methods that are readily adaptable to new fabrication techniques. Particularly, they have high specific surface areas and abundant catalytic sites that guide uniform nucleation and deposition. The ultrahigh surface area also increases the area exposed to the electrolyte, resulting in significant formation of SEI and electrolyte consumption. In comparison with metal-based materials, their electrical conductivity is lower, and their mechanical strength is less satisfactory, which needs to be further improved.

2. Metal-based materials exhibit various advantages, including high electrical conductivity and structural and mechanical stability. However, it should be noted that the fabrication into a 3D architecture may damage the mechanical strength to a certain extent. In addition, large-scale fabrication is costly, and most metals with high density do not meet the energy and powder density requirements. To maximize the advantages of carbon and metal-based materials, they can also be built into metal-carbon hybrid electrode materials, that is, a carbon framework with metal particles modified on the surface or a carbon framework on a metallic substrate. For the carbon framework with metal-based nanoparticles, the 3D carbon framework can provide highly porous and interconnected conductive networks; the metallic nanoparticles act as alkalic affinity sites to decrease the nucleation barrier and guide uniform K metal plating/stripping. For a metal substrate with carbon materials on the surface, the bottom metal substrate is highly electrically conductive and mechanically stable, supporting the top carbon layer with a large surface area. This is feasible for large-scale electrode fabrication, although it is unfeasible in terms of energy density.

3. MXene electrode materials with 2D structures exhibit high electrical/ionic conductivities, large surface areas, and rich functional groups with alkaline metal affinity. Therefore, they can be fabricated into 3D architectures and assembled using various substrates as alkaline metal anodes. Currently, its application as an alkali metal anode is still in its early stages owing to various challenges. For instance, the restacking issue of MXene nanosheets significantly limits their exposed area and nucleation sites. The mass production of MXenes remains a challenge, and most of the research on MXene-based electrode materials has been conducted on coin-type cells, which differs significantly from practical applications. Composite anodes composed of MXene/metallic materials or MXene/carbonate materials are expected to be a promising avenue for further development of MXene-based electrode materials.

Compared with Li/Na metal anodes, the investigation and development of K metal anodes are still in their early stage. However, the differences between K metal and Li/Na metal anodes should be clearly noted for their development. The K atom exhibits significantly higher reactivity and larger ionic radius than the Li and Na atoms, resulting in a more serious challenge for the K metal anode. Therefore, research on K metal anodes should focus on decreasing their reactivity and volumetric changes during plating/stripping. This calls for more comprehensive strategies, not only a rationally designed 3D host coupled with a stable interface layer but also in combination with electrolyte modulation, separator design, and other possible solutions to improve performance. In addition, to further promote the progress of K metal anodes, the following perspectives and challenges were proposed, indicating the need for additional research efforts:

1. For a metal-based current collector, a low-cost and lightweight Al foil can be used for K metal anode applications because K does not react with Al to form an alloy. Therefore, the rich host-modification experience of the Cu foil can provide valuable guidance in the rational design of Al-metal-based current collectors. The carbonaceous current collector for K metal anodes exhibits advantages from various aspects, such as light weight, versatile structure, and easy synthesis. However, its mechanical strength is unsatisfactory and needs to be improved to sustain long-term cycling or harsh working conditions.

2. For the material selection and functional modification of the current collector, most of the recently published studies are based on experimental trial-and-error in the laboratory and lack theoretical instructions. Therefore, it is highly promising and effective to apply appropriate simulation methods, such as high-throughput, to screen the optimized (metallic or carbonaceous) materials and estimate their material-structure-property relationships.

3. The 3D hosts of the K metal anode have large specific surface areas, which decreases the local current density to induce uniform K deposition and simultaneously causes significant electrolyte consumption. In addition, the large porosity is beneficial for metallic K accommodation and efficient charge transportation; however, it results in poor mechanical strength. Therefore, it is ideal to develop a protective interface layer to reduce the overuse of electrolytes. The mechanical strength of the 3D host should be further improved, striving for a balance between mechanical stability and accommodation capability.

4. The fundamental understanding of the mechanism of K metal anodes is limited, and an in-depth investigation is required. Investigation of the current advanced *in situ* and *ex situ* characterization techniques and post-mortem analyses to reveal the fundamental processes, such as the evolution of the SEI and K nucleation and growth behaviors, will provide valuable guidance for rational electrode design and effective dendrite suppression.

5. The most recently applied electrode designs or synthetic methods are complex, cost-effective, and barely compatible with the current battery industry applications. This calls for the simplification and manufacturing cost reduction of the electrode synthesis process to make it more easily accessible for practical applications.

The K metal shows great promise as an anode for metal batteries, which are considered to be advanced metal batteries beyond Li metal batteries. Therefore, the K metal anode is undoubtedly an attractive and hot research topic for next-generation battery technique, although several challenges still need to be overcome. We hope that this study will be helpful for researchers in this field in the rational design and development of K metal anodes.

DECLARATIONS

Authors' contributions

Conceived the manuscript: Liu D, Cai X
Wrote the manuscript: Liu D
Discussion of the manuscript: Shen J, Jian Z, Cai X
Reviewed the manuscript: Cai X

Availability of data and materials

Not applicable.

Financial support and sponsorship

This work was supported by the Natural Science Foundation of China (No. 22105129), Guangdong Basic and Applied Basic Research Foundation (No. 2022A1515011048), and the Science and Technology Innovation Commission of Shenzhen (No. JCYJ20200109105618137).

Conflicts of interest

All authors declared that there are no conflicts of interest.

Ethical approval and consent to participate.

Not applicable.

Consent for publication

Not applicable.

REFERENCES

1. Armand M, Tarascon JM. Building better batteries. *Nature* 2008;451:652-7. DOI PubMed
2. Dunn B, Kamath H, Tarascon JM. Electrical energy storage for the grid: a battery of choices. *Science* 2011;334:928-35. DOI PubMed
3. Service RF. Lithium-ion battery development takes Nobel. *Science* 2019;366:292. DOI PubMed
4. Li M, Lu J, Chen Z, Amine K. 30 years of lithium-ion batteries. *Adv Mater* 2018;30:1800561. DOI
5. Goodenough JB, Kim Y. Challenges for rechargeable Li batteries. *Chem Mater* 2010;22:587-603. DOI
6. Tao Y, Rahn CD, Archer LA, You F. Second life and recycling: energy and environmental sustainability perspectives for high-performance lithium-ion batteries. *Sci Adv* 2021;7:eabi7633. DOI PubMed PMC
7. Eshetu GG, Zhang H, Judez X, et al. Production of high-energy Li-ion batteries comprising silicon-containing anodes and insertion-type cathodes. *Nat Commun* 2021;12:5459. DOI PubMed PMC
8. Kwak WJ, Rosy, Sharon D, et al. Lithium-oxygen batteries and related systems: potential, status, and future. *Chem Rev* 2020;120:6626-83. DOI
9. Seh ZW, Sun Y, Zhang Q, Cui Y. Designing high-energy lithium-sulfur batteries. *Chem Soc Rev* 2016;45:5605-34. DOI PubMed
10. Grey CP, Hall DS. Prospects for lithium-ion batteries and beyond-a 2030 vision. *Nat Commun* 2020;11:6279. DOI PubMed PMC
11. Nitta N, Wu F, Lee JT, Yushin G. Li-ion battery materials: present and future. *Mater Today* 2015;18:252-64. DOI
12. Teng W, Wu J, Liang Q, et al. Designing advanced liquid electrolytes for alkali metal batteries: principles, progress, and perspectives. *Energy Environ Mater* 2023;6:e12355. DOI
13. Sun Y, Liu N, Cui Y. Promises and challenges of nanomaterials for lithium-based rechargeable batteries. *Nat Energy* 2016;1:16071. DOI
14. Rajagopalan R, Tang Y, Ji X, Jia C, Wang H. Advancements and challenges in potassium ion batteries: a comprehensive review. *Adv Funct Mater* 2020;30:1909486. DOI
15. Wu J, Lin C, Liang Q, et al. Sodium-rich NASICON-structured cathodes for boosting the energy density and lifespan of sodium-free-anode sodium metal batteries. *InfoMat* 2022;4:e12288. DOI
16. Zhao Y, Adair KR, Sun X. Recent developments and insights into the understanding of Na metal anodes for Na-metal batteries. *Energy Environ Sci* 2018;11:2673-95. DOI
17. Eftekhari A. Potassium secondary cell based on prussian blue cathode. *J Power Sources* 2004;126:221-8. DOI
18. Zhang W, Liu Y, Guo Z. Approaching high-performance potassium-ion batteries via advanced design strategies and engineering. *Sci Adv* 2019;5:eaav7412. DOI PubMed PMC
19. Zhang Q, Wang Z, Zhang S, Zhou T, Mao J, Guo Z. Cathode materials for potassium-ion batteries: current status and perspective. *Electrochem Energy Rev* 2018;1:625-58. DOI
20. Zhu Y, Yang X, Sun T, et al. Recent progresses and prospects of cathode materials for non-aqueous potassium-ion batteries. *Electrochem Energy Rev* 2018;1:548-66. DOI
21. Zhong F, Wang Y, Li G, et al. Beyond-carbon materials for potassium ion energy-storage devices. *Renew Sustain Energy Rev* 2021;146:111161. DOI
22. Tian Y, Li H, Zhang S, et al. Polymer "tape" -assisted ball-milling method fabrication few-atomic-layered bismuth for improving K^+ / Na^+ storage. *Energy Environ Mater* 2021;4:421-7. DOI
23. Guo Y, Li H, Zhai T. Reviving lithium-metal anodes for next-generation high-energy batteries. *Adv Mater* 2017;29:1700007. DOI

24. Lin D, Liu Y, Cui Y. Reviving the lithium metal anode for high-energy batteries. *Nat Nanotechnol* 2017;12:194-206. DOI PubMed
25. Popovic J. Review-recent advances in understanding potassium metal anodes. *J Electrochem Soc* 2022;169:030510. DOI
26. Dhir S, Wheeler S, Capone I, Pasta M. Outlook on K-ion batteries. *Chem* 2020;6:2442-60. DOI
27. Xiang J, Yang L, Yuan L, et al. Alkali-metal anodes: from lab to market. *Joule* 2019;3:2334-63. DOI
28. Hu L, Deng J, Liang Q, et al. Engineering current collectors for advanced alkali metal anodes: a review and perspective. *EcoMat* 2023;5:e12269. DOI
29. Liu H, Cheng X, Jin Z, et al. Recent advances in understanding dendrite growth on alkali metal anodes. *Energy Chem* 2019;1:100003. DOI
30. Zhong Y, Zhou S, He Q, Pan A. Architecture design principles for stable electrodeposition behavior-towards better alkali metal (Li/Na/K) anodes. *Energy Stor Mater* 2022;45:48-73. DOI
31. Yasin G, Arif M, Mehtab T, et al. Understanding and suppression strategies toward stable Li metal anode for safe lithium batteries. *Energy Stor Mater* 2020;25:644-78. DOI
32. Wang H, Yu D, Kuang C, et al. Alkali metal anodes for rechargeable batteries. *Chem* 2019;5:313-38. DOI
33. Liu B, Zhang J, Xu W. Advancing lithium metal batteries. *Joule* 2018;2:833-45. DOI
34. Zhang JG, Xu W, Xiao J, Cao X, Liu J. Lithium metal anodes with nonaqueous electrolytes. *Chem Rev* 2020;120:13312-48. DOI
35. Fan L, Ma R, Zhang Q, Jia X, Lu B. Graphite anode for a potassium-ion battery with unprecedented performance. *Angew Chem Int Ed* 2019;58:10500-5. DOI PubMed
36. Liu S, Mao J, Zhang L, Pang WK, Du A, Guo Z. Manipulating the solvation structure of nonflammable electrolyte and interface to enable unprecedented stability of graphite anodes beyond 2 years for safe potassium-ion batteries. *Adv Mater* 2021;33:2006313. DOI PubMed
37. Mao J, Wang C, Lyu Y, et al. Organic electrolyte design for practical potassium-ion batteries. *J Mater Chem A* 2022;10:19090-106. DOI
38. Liang HJ, Gu ZY, Zhao XX, et al. Advanced flame-retardant electrolyte for highly stabilized K-ion storage in graphite anode. *Sci Bull* 2022;67:1581-8. DOI
39. Li NW, Yin YX, Yang CP, Guo YG. An artificial solid electrolyte interphase layer for stable lithium metal anodes. *Adv Mater* 2016;28:1853-8. DOI PubMed
40. Bao C, Wang B, Liu P, et al. Solid electrolyte interphases on sodium metal anodes. *Adv Funct Mater* 2020;30:2004891. DOI
41. Luo Z, Qiu X, Liu C, et al. Interfacial challenges towards stable Li metal anode. *Nano Energy* 2021;79:105507. DOI
42. Zhao Y, Ye Y, Wu F, Li Y, Li L, Chen R. Anode interface engineering and architecture design for high-performance lithium-sulfur batteries. *Adv Mater* 2019;31:1806532. DOI
43. Liu W, Liu P, Mitlin D. Review of emerging concepts in SEI analysis and artificial SEI membranes for lithium, sodium, and potassium metal battery anodes. *Adv Energy Mater* 2020;10:2002297. DOI
44. Park S, Jin HJ, Yun YS. Advances in the design of 3D-structured electrode materials for lithium-metal anodes. *Adv Mater* 2020;32:2002193. DOI
45. Luo G, Liu D, Zhao J, et al. Negatively charged holey titania nanosheets added electrolyte to realize dendrite-free lithium metal battery. *Small* 2023;19:2206176. DOI
46. Luo G, Yin X, Liu D, Hussain A, Liu F, Cai X. Electrosynthesis of vertically aligned zinc oxide nanoflakes on 3D porous Cu foam enables dendrite-free Li-metal anode. *ACS Appl Mater Interfaces* 2022;14:33400-9. DOI PubMed
47. Liu D, Wang Y, Tong T, Luo G, Shen J, Cai X. Mesoporous copper-based metal glass as current collector for Li metal anode. *Chem Eng J* 2023;451:138910. DOI
48. Zheng ZJ, Ye H, Guo ZP. Recent progress in designing stable composite lithium anodes with improved wettability. *Adv Sci* 2020;7:2002212. DOI PubMed PMC
49. Wu J, Chen X, Fan W, Li X, Mai Y, Chen Y. Rationally designed alloy phases for highly reversible alkali metal batteries. *Energy Stor Mater* 2022;48:223-43. DOI
50. Wu F, Yuan Y, Cheng X, et al. Perspectives for restraining harsh lithium dendrite growth: towards robust lithium metal anodes. *Energy Stor Mater* 2018;15:148-70. DOI
51. Hussain A, Mehmood A, Saleem A, et al. Polyetherimide membrane with tunable porous morphology for safe lithium metal-based batteries. *Chem Eng J* 2023;453:139804. DOI
52. Raza W, Hussain A, Mehmood A, et al. Poly(ether imide) porous membrane developed by a scalable method for high-performance lithium-sulfur batteries: combined theoretical and experimental study. *ACS Appl Mater Interfaces* 2022;14:52794-805. DOI
53. Wei C, Tao Y, An Y, et al. Recent advances of emerging 2D MXene for stable and dendrite-free metal anodes. *Adv Funct Mater* 2020;30:2004613. DOI
54. Chen J, Wang Y, Li S, et al. Porous metal current collectors for alkali metal batteries. *Adv Sci* 2022;10:2205695. DOI PubMed PMC
55. Wei C, Tao Y, Fei H, et al. Recent advances and perspectives in stable and dendrite-free potassium metal anodes. *Energy Stor Mater* 2020;30:206-27. DOI
56. Liu P, Mitlin D. Emerging potassium metal anodes: perspectives on control of the electrochemical interfaces. *ACC Chem Res* 2020;53:1161-75. DOI PubMed
57. Shi P, Zhang X, Shen X, Zhang R, Liu H, Zhang Q. A review of composite lithium metal anode for practical applications. *Adv Mater*

Technol 2020;5:1900806. DOI
58. Yang G, Li Y, Tong Y, et al. Lithium plating and stripping on carbon nanotube sponge. *Nano Lett* 2019;19:494-9. DOI
59. Zuo TT, Wu XW, Yang CP, et al. Graphitized carbon fibers as multifunctional 3D current collectors for high areal capacity Li anodes. *Adv Mater* 2017;29:1700389. DOI
60. Pan L, Luo Z, Zhang Y, et al. Seed-free selective deposition of lithium metal into tough graphene framework for stable lithium metal anode. *ACS Appl Mater Interfaces* 2019;11:44383-9. DOI
61. Niu C, Pan H, Xu W, et al. Self-smoothing anode for achieving high-energy lithium metal batteries under realistic conditions. *Nat Nanotechnol* 2019;14:594-601. DOI
62. Cui J, Yao S, Ihsan-ul-haq M, Wu J, Kim J. Correlation between Li Plating behavior and surface characteristics of carbon matrix toward stable Li metal anodes. *Adv Energy Mater* 2019;9:1802777. DOI
63. Chen X, Chen XR, Hou TZ, et al. Lithiophilicity chemistry of heteroatom-doped carbon to guide uniform lithium nucleation in lithium metal anodes. *Sci Adv* 2019;5:eaau7728. DOI PubMed PMC
64. Zhang C, Liu S, Li G, Zhang C, Liu X, Luo J. Incorporating ionic paths into 3D conducting scaffolds for high volumetric and areal capacity, high rate lithium-metal anodes. *Adv Mater* 2018;30:1801328. DOI
65. Li S, Liu Q, Zhou J, et al. Hierarchical Co_3O_4 nanofiber-carbon sheet skeleton with superior Na/Li-philic property enabling highly stable alkali metal batteries. *Adv Funct Mater* 2019;29:1808847. DOI
66. Li Y, Zhang L, Liu S, et al. Original growth mechanism for ultra-stable dendrite-free potassium metal electrode. *Nano Energy* 2019;62:367-75. DOI
67. Qin L, Lei Y, Wang H, et al. Capillary encapsulation of metallic potassium in aligned carbon nanotubes for use as stable potassium metal anodes. *Adv Energy Mater* 2019;9:1901427. DOI
68. Ye M, Hwang JY, Sun YK. A 4 V class potassium metal battery with extremely low overpotential. *ACS Nano* 2019;13:9306-14. DOI PubMed
69. Meng J, Zhu H, Xiao Z, et al. Amine-wetting-enabled dendrite-free potassium metal anode. *ACS Nano* 2022;16:7291-300. DOI
70. Zhang D, Ma X, Wu L, et al. Coupling low-tortuosity carbon matrix with single-atom chemistry enables dendrite-free potassium-metal anode. *Adv Energy Mater* 2023;13:2203277. DOI
71. Yang Y, Huang C, Zhang Y, et al. Processable potassium-carbon nanotube film with a three-dimensional structure for ultrastable metallic potassium anodes. *ACS Appl Mater Interfaces* 2022;14:55577-86. DOI
72. Cheng G, Liu S, Wang X, et al. CoZn nanoparticles@hollow carbon tubes enabled high-performance potassium metal batteries. *ACS Appl Mater Interfaces* 2022;14:45364-72. DOI
73. Zhang J, Li Y, Zhu L, Wang X, Tu J. Potassiophilic skeleton achieving highly stable potassium metal anode. *Chem Eng J* 2022;449:137659. DOI
74. Wang L, Wang H, Cheng M, et al. Metal-organic framework@polyacrylonitrile-derived potassiophilic nanoporous carbon nanofiber paper enables stable potassium metal anodes. *ACS Appl Energy Mater* 2021;4:6245-52. DOI
75. Xie Y, Hu J, Han Z, et al. Ultra-stable K metal anode enabled by oxygen-rich carbon cloth. *Nano Res* 2020;13:3137-41. DOI
76. Zhou M, Qi W, Hu Z, et al. Highly potassiophilic carbon nanofiber paper derived from bacterial cellulose enables ultra-stable dendrite-free potassium metal anodes. *ACS Appl Mater Interfaces* 2021;13:17629-38. DOI
77. Qiao F, Meng J, Wang J, et al. Building carbon cloth-based dendrite-free potassium metal anodes for potassium metal pouch cells. *J Mater Chem A* 2021;9:23046-54. DOI
78. Zhao X, Chen F, Liu J, et al. Enhanced surface binding energy regulates uniform potassium deposition for stable potassium metal anodes. *J Mater Chem A* 2020;8:5671-8. DOI
79. Liu S, Yang Y, Qian Y, et al. MOF-derived potassiophilic CuO nanoparticles on carbon fiber cloth as host for stabilizing potassium metal anode. *ChemElectroChem* 2022;9:e202101561. DOI
80. Han M, Jiang J, Lu S, et al. Moderate specific surface areas help three-dimensional frameworks achieve dendrite-free potassium-metal anodes. *ACS Appl Mater Interfaces* 2022;14:900-9. DOI
81. Yang CP, Yin YX, Zhang SF, Li NW, Guo YG. Accommodating lithium into 3D current collectors with a submicron skeleton towards long-life lithium metal anodes. *Nat Commun* 2015;6:8058. DOI PubMed PMC
82. Yun Q, He YB, Lv W, et al. Chemical dealloying derived 3D porous current collector for Li metal anodes. *Adv Mater* 2016;28:6932-9. DOI
83. Li Q, Zhu S, Lu Y. 3D porous Cu current collector/Li-metal composite anode for stable lithium-metal batteries. *Adv Funct Mater* 2017;27:1606422. DOI
84. Wang X, Zeng W, Hong L, et al. Stress-driven lithium dendrite growth mechanism and dendrite mitigation by electroplating on soft substrates. *Nat Energy* 2018;3:227-35. DOI
85. Lee J, Won ES, Kim DM, et al. Three-dimensional porous frameworks for Li metal batteries: superconformal versus conformal Li growth. *ACS Appl Mater Interfaces* 2021;13:33056-65. DOI
86. Chen J, Li S, Qiao X, et al. Integrated porous Cu host induced high-stable bidirectional Li plating/stripping behavior for practical Li metal batteries. *Small* 2022;18:2105999. DOI
87. Wang T, Liu Y, Lu Y, Hu Y, Fan L. Dendrite-free Na metal plating/stripping onto 3D porous Cu hosts. *Energy Stor Mater* 2018;15:274-81. DOI
88. Chu C, Li R, Cai F, et al. Recent advanced skeletons in sodium metal anodes. *Energy Environ Sci* 2021;14:4318-40. DOI

89. Yang W, Yang W, Dong L, Shao G, Wang G, Peng X. Hierarchical ZnO nanorod arrays grown on copper foam as an advanced three-dimensional skeleton for dendrite-free sodium metal anodes. *Nano Energy* 2021;80:105563. DOI
90. Wang C, Wang H, Matios E, Hu X, Li W. A chemically engineered porous copper matrix with cylindrical core-shell skeleton as a stable host for metallic sodium anodes. *Adv Funct Mater* 2018;28:1802282. DOI
91. Chen Q, Liu B, Zhang L, et al. Sodiophilic Zn/SnO_2 porous scaffold to stabilize sodium deposition for sodium metal batteries. *Chem Eng J* 2021;404:126469. DOI
92. Liu P, Wang Y, Gu Q, Nanda J, Watt J, Mitlin D. Dendrite-free potassium metal anodes in a carbonate electrolyte. *Adv Mater* 2020;32:1906735. DOI
93. Wang J, Yuan J, Chen C, et al. Cu_3Pt alloy-functionalized Cu mesh as current collector for dendritic-free anodes of potassium metal batteries. *Nano Energy* 2020;75:104914. DOI
94. Wang J, Yan W, Zhang J. High area capacity and dendrite-free anode constructed by highly potassiophilic Pd/Cu current collector for low-temperature potassium metal battery. *Nano Energy* 2022;96:107131. DOI
95. Li H, Liu Y, Wang J, Yan W, Zhang J. Robust 3D copper foam functionalized with gold nanoparticles as anode for high-performance potassium metal batteries. *Chem Asian J* 2022;17:e202200430. DOI
96. Liu F, Wang L, Ling F, et al. Homogeneous metallic deposition regulated by porous framework and selenization interphase toward stable sodium/potassium anodes. *Adv Funct Mater* 2022;32:2210166. DOI
97. Liu P, Wang Y, Hao H, et al. Stable potassium metal anodes with an all-aluminum current collector through improved electrolyte wetting. *Adv Mater* 2020;32:2002908. DOI
98. Yi Y, Li J, Gao Z, et al. Highly potassiophilic graphdiyne skeletons decorated with Cu quantum dots enable dendrite-free potassium-metal anodes. *Adv Mater* 2022;34:2202685. DOI
99. Ye S, Wang L, Liu F, Shi P, Yu Y. Integration of homogeneous and heterogeneous nucleation growth via 3D alloy framework for stable Na/K metal anode. *eScience* 2021;1:75-82. DOI
100. Shi H, Dong Y, Zheng S, Dong C, Wu ZS. Three dimensional Ti_3C_2 MXene nanoribbon frameworks with uniform potassiophilic sites for the dendrite-free potassium metal anodes. *Nanoscale Adv* 2020;2:4212-9. DOI PubMed PMC
101. Shi H, Yue M, Zhang CJ, et al. 3D Flexible, Conductive, and Recyclable $Ti_3C_2T_x$ MXene-melamine foam for high-areal-capacity and long-lifetime alkali-metal anode. *ACS Nano* 2020;14:8678-88. DOI
102. Tang X, Zhou D, Li P, et al. MXene-based dendrite-free potassium metal batteries. *Adv Mater* 2020;32:1906739. DOI
103. Fang Y, Zhang Y, Zhu K, et al. Lithiophilic three-dimensional porous $Ti_3C_2T_x$-rGO membrane as a stable scaffold for safe alkali metal (Li or Na) anodes. *ACS Nano* 2019;13:14319-28. DOI
104. Pang J, Mendes RG, Bachmatiuk A, et al. Applications of 2D MXenes in energy conversion and storage systems. *Chem Soc Rev* 2019;48:72-133. DOI